Feasibility of using vessel-detection software for the endovascular treatment of visceral arterial bleeding

Jin Iwazawa, Shoichi Ohue, Naoko Hashimoto, Takashi Mitani

Abstract
We aimed to investigate the feasibility of using vessel-detection software to identify damaged arteries during endovascular embolization in five patients with visceral arterial hemorrhages. We used a software program originally developed to detect tumor feeder vessels in liver tumor embolization with C-arm computed tomography datasets to detect the vessels responsible for the arterial hemorrhages in patients with splenic artery pseudoaneurysms (n=2), lower gastrointestinal bleeding (n=2), and bladder tumor bleeding (n=1). In all cases, the injured vessel was identified accurately on a three-dimensional vascular map at the optimal working angle with a relatively short mean processing time of 118 s (range, 107–136 s). The operating angiographers used this information to direct the catheter into the damaged artery without sequential angiographic runs. The software analysis was also used to plan coil delivery to the most appropriate site in the injured artery. The results suggest that the vessel-detection software for liver tumor embolization can also be used to detect damaged vessels and to plan treatment strategies in endovascular embolization of visceral arterial hemorrhage.

Endovascular embolization for arterial hemorrhage of visceral organs is an established treatment for managing hemodynamically unstable patients (1, 2). Accurate, prompt identification of the damaged artery during the treatment session is essential for timely control of hemorrhage. However, sequential angiographic runs are usually necessary for the manual identification of the leaking artery on two-dimensional (2D) angiographic images. Recently, computer software specifically designed to assist in planning liver tumor embolization (FlightPlan for Liver, GE Healthcare, Waukesha, Wisconsin, USA) was developed (3). This software predicts tumor feeder vessels automatically and provides a three-dimensional (3D) image with a single acquisition with nonselective C-arm computed tomography (CT). Studies have demonstrated that the software showed better sensitivity (approximately 90%) for detecting tumor feeders with a shorter processing time (approximately 2 min) than manual angiographic assessments (3–6).

This article describes our initial attempts at using the vessel-detection software to identify the vessels responsible for arterial bleeding during endovascular embolization in five patients with visceral arterial hemorrhages.

Materials and methods

Patients

We performed transcatheter arterial embolization with the aid of vessel-detection software (FlightPlan for Liver, GE Healthcare) in five patients (mean age, 52 years; range, 30–88 years) with arterial hemorrhages of visceral organs seen between March 2012 and May 2013. The causes of the arterial hemorrhages were pseudoaneurysms of the splenic artery due to acute pancreatitis (n=2), diverticulitis of the colon (n=1), jejunal bleeding of unknown origin (n=1), and bleeding from a bladder tumor (n=1). Angiography and C-arm CT performed during the endovascular procedure confirmed the diagnosis of hemorrhage. This study proceeded in accordance with the guidelines of the Institutional Review Board of Nissay Hospital, and written informed consent for endovascular treatment using the software was obtained from each patient.

Vessel detection using the software

The angiographic procedures were performed using a flat-panel detector C-arm angiographic system (Innova 3100, GE Healthcare). The arteries responsible for bleeding were detected using vessel-detection software (FlightPlan for Liver) during an angiographic session. Under the supervision of board-certified interventional radiologists (J.I. and S.O.), a single radiology technologist performed the image analyses re-

From the Deparment of Radiology (J.I. ✉ *iwazawa.jin@nissay-hp. or.jp*, N.H., T.M.), Nissay Hospital, Osaka, Japan; the Department of Radiology (S.O.), Komatsu Hospital, Neyagawa, Japan.

Table. Demographic and treatment profiles of patients with visceral arterial hemorrhages who underwent endovascular embolization using vessel-detection software

Patient number	Gender, age (years)	Etiology	Damaged artery	Embolus	Technical outcome	Software prediction	DSA acquisitions	C-arm CT acquisitions	Procedural time (min)	Software processing time (s)
1	M, 37	Acute pancreatitis	Splenic	Coil	Success	Correct	3	2	135	112
2	F, 88	Unknown	Jejunal	Coil	Success	Correct	4	2	55	128
3	M, 30	Diverticulitis	Right colic	Coil	Success	Correct	4	1	105	136
4	M, 57	Acute pancreatitis	Splenic	Coil	Success	Correct	3	2	137	110
5	F, 48	Bladder tumor	Superior vesical	Gelatin sponge	Success	Correct	4	2	70	107

C-arm CT, C-arm computed tomography; DSA, digital subtraction angiography; F, female; M, male.

lated to vessel detection on the same commercial workstation (Advantage Workstation 5.0, GE Healthcare) to minimize interoperator variability. Nonselective C-arm CT data for the examined artery were obtained with the following acquisition parameters: total scanning angle, 200°; rotation speed, 40°/s; acquisition time, 5 s; matrix size, 1500×1500; isotropic voxel size, 0.2 mm; and effective field-of-view, 18 cm^2. Data acquisition was started 7–8 s after an intra-arterial injection of contrast medium, and the volume datasets were transferred to an external workstation (Advantage Workstation 5.0) automatically. After the technologist had selected the catheter entry site on the volume-rendered C-arm CT image on the workstation, the entire arterial vasculature of the examined artery was extracted as a circumscribed image in approximately 15 s. Subsequently, the operating angiographers detected extravasation on the multisectional C-arm CT images in consensus. Then, the radiology technologist placed a circular region-of-interest (ROI) to cover the entire bleeding site using 2D-multiplanar reformatted (MPR) images. With the extraction function of the software, the damaged artery connecting the selected catheter entry site to the bleeding site was highlighted on volume-rendered images in approximately 30 s. The arteries responsible for bleeding were determined by the software on the basis of a model in which all bleeding regions are supplied by their closest vessels (3).

Endovascular embolization

To treat the splenic artery pseudoaneurysm, a 2.7 F microcatheter (Sniper II, Terumo, Tokyo, Japan) was inserted into the proximal splenic artery coaxially through a 5 F catheter. C-arm CT images of the splenic artery were obtained by injecting 10 mL of iopamidol (Iopamiron 370, Bayer Schering Pharma, Osaka, Japan) at a flow rate of 1.0 mL/s. After the pseudoaneurysm was confirmed on the C-arm CT image, the origin of the bleeding was determined using the software. The pseudoaneurysm was isolated using microcoils (Tornado Platinum Microcoils, Cook Medical, Bloomington, Indiana, USA).

To control the bladder hemorrhage, a pelvic artery angiogram was first obtained using a 5 F pigtail catheter placed in the abdominal aorta. Then, a 4 F curved-tip catheter was advanced into the right common iliac artery. C-arm CT images of the right common iliac artery were obtained by injecting 30 mL of iopamidol at a flow rate of 3.0 mL/s. The software analysis indicated that the superior vesical artery was the source of the bleeding. Therefore, a 4 F catheter was advanced into the artery directly. A selective angiogram of this artery was acquired during contrast injection to confirm that the vessel was the source of the bleeding. The artery was embolized with gelatin particles (Gelpart, Nippon Kayaku, Tokyo, Japan).

To manage the lower intestinal bleeding, C-arm CT images of the superior mesenteric artery were acquired by injecting 25 mL of iopamidol at a flow rate of 2.5 mL/s. To reduce peristalsis, 20 mg of scopolamine butylbromide (Buscopan, Nippon Boehringer Ingelheim, Tokyo, Japan) were administered intravenously before image acquisition. First, the angiographers identified the bleeding site using the C-arm CT image acquired during contrast injection of the superior mesenteric artery. Then, the radiology technologist placed a circular ROI on the bleeding site using 2D-MPR C-arm CT images. The software subsequently identified the damaged artery, connecting the selected catheter entry site to the bleeding site and displayed highlighted 3D images. Then, a 1.7 F microcatheter (Cross I, Piorax Medical Devices, Yokohama, Japan) was inserted coaxially into the vasa recta suggested by the software analysis. The outer diameter of the microcatheter at the distal radiopaque marker is 1.9 F, but the tip of the catheter tapers to 1.7 F. A selective angiogram of the vasa recta was obtained to confirm the bleeding, and the vasa recta was subsequently occluded using microcoils (Tornado Platinum Microcoils, Cook Medical).

Results

The patient and treatment profiles for the five cases are summarized in Table. All bleeding sites were detected on both the C-arm CT and angiographic images. The software predicted the artery responsible for the bleeding precisely, and endovascular treatment using vessel-detection software for visceral bleeding was successful in all cases. Creation of an arterial shortcut at the hairpin turn in a single artery was observed in one of the cases (Fig. 1). The mean number of angiography and C-arm CT acquisitions in a single session was 3.6 (range, 3–4) and 1.8 (range, 1–2), respectively. The mean overall procedure time was 100 min (range, 55–137 min). The mean total processing time required from the

time the C-arm CT image was available to the operator to when the software completed vessel extraction was 118 s (range, 107–136 s). Representative cases are shown in Figs. 1 and 2.

Discussion

In endovascular therapy, urgent identification of the damaged artery is required for prompt control of arterial bleeding. However, manual angiographic assessment is relatively time consuming because sequential angiographic image acquisitions are usually necessary to identify the leaking artery, and determination of the specific artery responsible for the bleeding is difficult when the arterial vasculature has a complex branching pattern. The application of vessel-detection software in the endovascular treatment of arterial hemorrhage should reduce the number of image acquisitions and the overall procedure time, because the software can identify a damaged vessel from nonselective C-arm CT arteriography images, and facilitate direct placement of a microcatheter into the culprit vessel without the need for sequential angiography. Further, the software visualizes the arterial path from the catheter tip to the target site on a 3D vascular map at the optimal working angle, enabling easier, quicker, and more accurate targeted catheterization.

This study demonstrated that vessel-detection software for liver tumors could be applied to endovascular treatment for arterial bleeding from abdominal organs. When treating pseudoaneurysms, the software could identify the origin of the bleeding in terms of the parent artery and aneurysm itself. Such 3D visualization facilitated preoperative treatment planning. The optimal delivery point of the platinum coil was determined accurately, and both the bleeding point and arterial route from the catheter to the target were visualized simultaneously on 3D
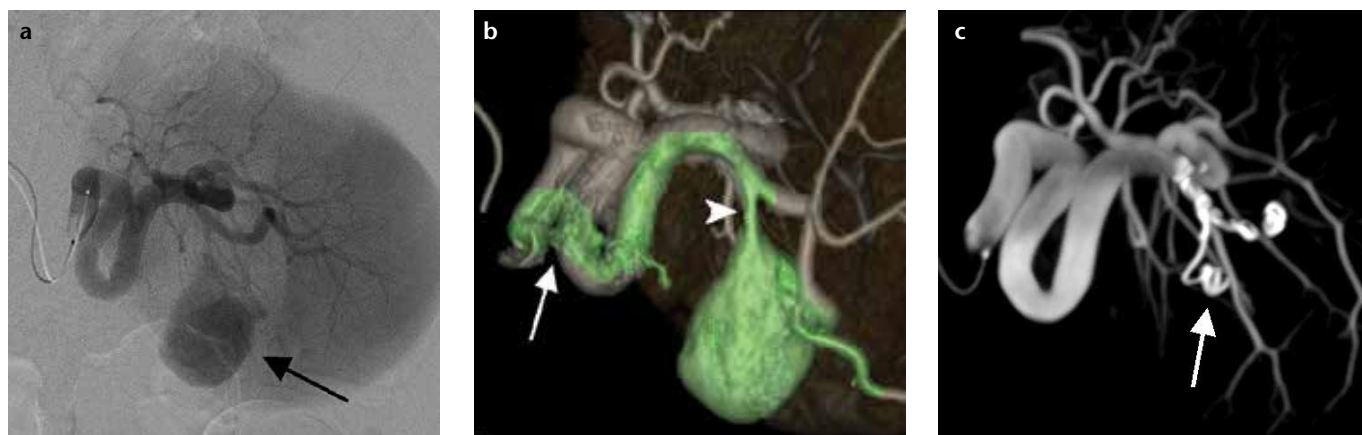

Figure 1. a–c. Images obtained from a 37-year-old male with a splenic artery pseudoaneurysm caused by acute pancreatitis who underwent endovascular treatment using vessel-detection software. The splenic artery angiogram **(a)** shows the target pseudoaneurysm *(arrow)*, but the exact origin, location, and vasculature of the damaged artery are not clear. The software analysis of the volume-rendered C-arm CT image of the splenic artery **(b)** indicates a single bleeding site *(arrowhead)* at the second branch of the splenic artery. The software indicates the arterial path from the catheter to the target aneurysm in green. Note the arterial shortcut created at the hairpin turn in a single artery *(arrow)*. The maximum intensity projection C-arm CT image **(c)** obtained after coil embolization of the parent artery *(arrow)* confirms disappearance of the pseudoaneurysm.
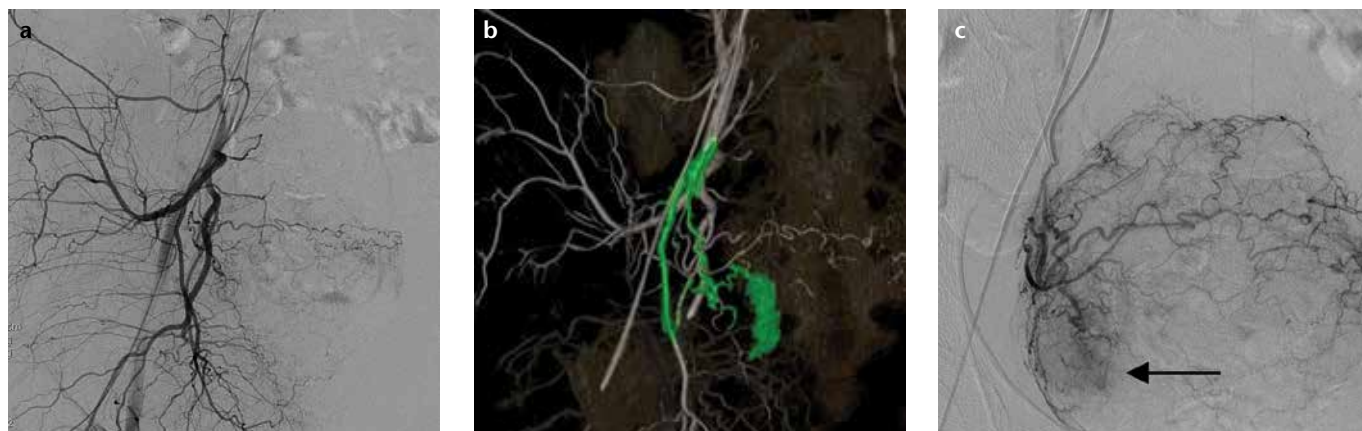

Figure 2. a–c. Images obtained from a 70-year-old female with bleeding from a bladder tumor undergoing transcatheter arterial embolization using vessel-detection software. The bleeding site is not visible on the right internal iliac artery angiogram **(a)**. The software analysis of the volume-rendered C-arm CT image of the right internal iliac artery **(b)** indicates that the superior vesical artery is responsible for the bladder hemorrhage, as indicated in green. Direct catheterization into the superior vesical artery **(c)** demonstrates extravasation *(arrow)* from the right side of the urinary bladder.

images from single nonselective C-arm CT datasets.

For prompt identification of the damaged artery, the processing time of the software should be as short as possible. In this study, the total processing time from the time the C-arm CT image became available to the radiology technologist to when the software identified the tumor feeder was approximately 2 min. This time is roughly comparable to the time required for manual angiographic assessment. Furthermore, whereas the angiographer assesses angiographic images manually during the treatment session, the radiology technologist can assess the vessels using the software, so the angiographer is not interrupted during the procedure. Moreover, sequential angiographic runs are not necessary when using the software to detect the culprit vessels.

In patients with multiple bleeding points, each responsible artery could be determined from a single acquisition of a nonselective C-arm CT image during contrast injection of the proximal artery. Multiple software processes are necessary to detect the artery responsible for each bleeding site. When the bleeding sites are distributed over multiple organs, multiple C-arm CT image acquisitions are required. Each responsible artery is highlighted as a colored vessel in separate volume-rendered images.

There are several fundamental limitations to using this software in en-dovascular therapy. Very fine arteries, especially their distal parts, were sometimes not extracted by the software during the initial extraction process (6). This failure might cause misinterpretation of the damaged artery. An irregular shape of the target hemorrhage might complicate the target-definition process, and incorrect target definition might cause misinterpretation by the software. Further, C-arm CT is more susceptible to patient motion than conventional CT. Transient movement during image acquisition negatively affects the quality of the entire image (7), and the resultant imaging data can result in the apparent fusion of nearby arteries, resulting in misinterpretation. Another limitation is that the field-of-view of this imaging technique is insufficient to cover the entire body. Such limitations might interfere with accurate identification of the vessels responsible for bleeding.

This study has its limitations. The number of patients was small. In addition, the bleeding points or vessels were relatively easy to detect in the cases presented here. Further investigations involving more cases are required to assess the utility of the vessel-detection software for the endovascular treatment of visceral bleeding.

In conclusion, the vessel-detection software for liver tumor embolization can also be used to guide endovascular embolization of visceral arterial hemorrhage by the accurate, rapid identification of damaged vessels.

References

1. Peck DJ, McLoughlin RF, Hughson MN, Rankin RN. Percutaneous embolotherapy of lower gastrointestinal hemorrhage. J Vasc Interv Radiol 1998; 9:747–751. [CrossRef]
2. Bergert H, Hinterseher I, Kersting S, Leonhardt J, Bloomenthal A, Saeger HD. Management and outcome of hemorrhage due to arterial pseudoaneurysms in pancreatitis. Surgery 2005; 137:323–328. [CrossRef]
3. Pichon E, Bekes G, Deschamps F, Solomon SB. Development and preliminary evaluation of software for planning selective liver embolizations from three-dimensional rotational fluoroscopy imaging. Int J Comput Assist Radiol Surg 2008; 3:405–412. [CrossRef]
4. Solomon SB, Thornton R, Deschamps F, et al. A treatment planning system for transcatheter hepatic therapies: pilot study. J Interv Oncol 2008; 1:12–18.
5. Deschamps F, Solomon SB, Thornton RH, et al. Computed analysis of three-dimensional cone-beam computed tomography angiography for determination of tumor-feeding vessels during chemoembolization of liver tumor: a pilot study. Cardiovasc Intervent Radiol 2010; 33:1235–1242. [CrossRef]
6. Iwazawa J, Ohue S, Hashimoto N, Muramoto O, Mitani T. Clinical utility and limitations of tumor-feeder detection software for liver cancer embolization. Eur J Radiol 2013; 82:1665–1671. [CrossRef]
7. Iwazawa J, Ohue S, Hashimoto N, Abe H, Hamuro M, Mitani T. Detection of hepatocellular carcinoma: comparison of angiographic C-arm CT and MDCT. AJR Am J Roentgenol 2010; 195:882–887. [CrossRef]